Shedding light on active species in Fe, Ni and Cu catalysis

Draksharapu, Apparao

Introduction

Raman spectroscopy and electrochemistry in the study of inorganic complexes of relevance to catalysis

A general introduction to the topics discussed in this thesis is presented in this chapter. The chapter has been divided into three parts. In the first part, a survey of the use of Raman spectroscopy as a tool for fingerprinting in the characterisation of iron and manganese based complexes involved in oxidation chemistry is presented. In the second part, the electrochemical properties of $Fe^{IV}=O$ *complexes are discussed. In the third part, biochemical halogenation reactions and their reaction pathways are reviewed.*

Parts of this chapter have been published:
J. J. McGarvey, A. Draksharapu, W. R. Browne, *Special Periodic Reports*, **2013**, *44*, 68-94.
C. Brennan, A. Draksharapu, W. R. Browne, J. J. McGarvey, J. G. Vos, M. T. Pryce, *Dalton Trans.*, **2013**, *42*, 2546-2555.

Chapter 1

I.1 Raman spectroscopy and its application in speciation of inorganic compounds

Detailed investigation of the vibrational and vibronic energy states under static conditions is important in the development of a more complete understanding of the structure of biological systems. In many cases these studies focus on their biological function and potential application in a catalytic context. This chapter selects a number of recent examples of the use of Raman and resonance Raman methods to probe a variety of metal-centred systems in biomimetic oxidation catalysts and focuses primarily on iron based systems of relevance to the work described in this thesis.

I.1.1 Introduction

The versatile chemical, photochemical and photophysical behaviour of metal complexes arising from the diverse range of electronic states accessed through several types of perturbation has stimulated increasing interest in metal-centred systems over the last decades. The manifold of states of various orbital types that are accessible in mono- and multi-nuclear metal complexes remains key to the continuing interest in their investigation. In mononuclear metal-centred species with a single type of ligand, the most common orbital transitions involved in thermal and photochemical excitation are generally metal-centred (MC), metal-ligand charge-transfer (MLCT), ligand-metal charge-transfer (LMCT) or possibly ligand-centred (LC). The focus of this chapter will be primarily on the use of Raman spectroscopy to extract detailed structural information. This concerns primarily catalytically important biomimetic complexes and recent studies that demonstrate the use of this technique in understanding second coordination sphere effects.

I.1.2 Methods for structural and dynamic investigation of electronic and vibrational levels in metal complexes

When light interacts with matter several things may happen. Light may pass through the sample without interacting with it, or it may be absorbed (UV/Vis and IR spectroscopy depending on the light source) or it may scatter (Rayleigh scattering and Raman spectroscopy). Raman spectroscopy is a complementary technique to IR spectroscopy. In principle both Raman and IR spectroscopy give the same information about a molecule but differ in their physical basis and selection rules. IR spectroscopy is an absorption spectroscopy, where the absorption of the incident IR radiation causes the excitation of the molecule to higher vibrational

levels. The excitation happens when the frequency of the light matches the energy difference between the vibrational levels. In contrast, Raman spectroscopy involves excitation, with monochromatic light, of the molecule to 'virtual states' from where the molecule relaxes to the same or different vibrational level compared to the initial state. Raman spectroscopy depends on the inelastic scattering of light when it interacts with matter. Scattering can be divided into two categories elastic scattering (Rayleigh scattering, the frequency of the scattered light is the same as the incident light) and inelastic scattering (the frequency of the scattered light is different compared to the incident light). Most of the light will scatter elastically, so it is not useful for Raman spectroscopy. Inelastic scattering occurs when the scattered light has a different frequency than that of the incident light. If the scattered light has a higher frequency than the incident light, it is referred to as anti-Stokes scattering. This is unlikely at room temperature because the molecule should be initially in a higher vibrational state. If the scattered light has a lower frequency than the incident light, it is referred to as Stokes scattering. It is common to measure Stokes scattering for practical reasons. Raman spectroscopy is inherently weak since approximately for one photon in every 10^6 - 10^7 photons will scatter inealistically.

The selection rules for IR and Raman spectroscopy are also different. A vibrational mode becomes IR active, if there is a change in dipole moment during that vibration, whereas Raman spectroscopy needs a change in the polarisability. For example, the symmetric and asymmetric vibrational mode of carbon dioxide are shown in Figure 1. In the symmetric vibrational modes there is no change in the dipole moment and, hence, this mode is IR inactive. However, a change in polarisability occurs during this vibration so this mode is Raman active, indeed a peak corresponding to this mode appears at 1335 cm^{-1}. In the case of the asymmetric vibrational mode, the rate of change in the polarisability at the mean is zero, hence, this mode is Raman inactive. But the dipole moment of the molecule changes in this vibration and IR absorption is observed at 2349 cm^{-1}. With the help of group theory it is possible to assign the Raman and IR active modes in a given molecule.

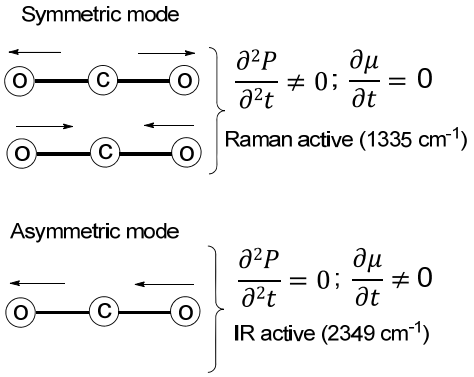

Figure 1 Symmetric and asymmetric vibrational modes of carbon dioxide. Where P is polarisability and μ is dipolemoment.

The frequency of the Raman or IR band frequency can be calculated using Hooke's law (equation 1)

$$\bar{\vartheta}\ (\mathrm{cm^{-1}}) = \frac{1}{2\pi c}\frac{\sqrt{K}}{\sqrt{\mu}} \qquad \text{.....equation 1}$$

Where ῡ wavenumber (cm^{-1}), c speed of light (2.997 x 10^{10} cm s^{-1}), K is the force constant (dynes cm^{-1} where dyne = g cm s^{-2}) and μ reduced mass ((M_1xM_2)/(M_1+ M_2) in grams).

From equation 1 it is clear that the stronger the bond the higher its vibrational frequency and *vice versa*. For example the vibrational frequencies of C≡C (2250 cm^{-1}) > C=C (1600 cm^{-1}) > C-C (1000 cm^{-1}). Furthermore, the lower the mass, the higher the vibrational frequency. For example $CHCl_3$ shows a C-H stretching band at 3021 cm^{-1}. If C-H is replaced with C-D, it is possible to predict the change in vibrational frequency from equation 2. A value $\bar{\upsilon}_{C\text{-}D}$ (2216 cm^{-1}) can be calculated upon substituting the values of $\bar{\upsilon}_{C\text{-}H}$ (3021 cm^{-1}), $\mu_{C\text{-}H}$ (0.92 g) and $\mu_{C\text{-}D}$ (1.71 g) in equation 2. Indeed, a band at 2254 cm^{-1} is observed experimentally in the Raman spectrum of $CDCl_3$.[1]

$$\frac{\bar{\upsilon}_1}{\bar{\upsilon}_2} = \frac{\sqrt{\mu_2}}{\sqrt{\mu_1}} \quad => \quad \bar{\upsilon}_2 = \bar{\upsilon}_1 \ \mathrm{x}\ \frac{\sqrt{\mu_1}}{\sqrt{\mu_2}} \qquad \text{.....equation 2}$$

Similarly, ^{18}O isotope labelling is often employed for the definitive assignments of intermediate such as Fe^{IV}=O, Fe^{III}-OOH, Fe^{III}-(OO), Fe^{III}-OCl and Mn^{IV}=O etc. However, as shown in chapter 6, definitive assignment of an Fe^{III}-O-Cl species was not possible even after labelling with ^{18}O. This is due to the similarity in predicted

shifts for Fe-O^{18} (29 cm^{-1}) and ^{18}O-Cl (26 cm^{-1}) calculated from Hooke's law under a two atom approximation. In this case exchange with a heavier atom such as bromine (Fe^{III}-O-Br) was employed to assign the vibrational modes of Fe^{III}-O and O-Cl (see chapter 6 for the details).

Due to the inherently weak nature of Raman scattering, high concentrations is needed to acquire a Raman spectrum in solution. Fortunately, this problem can overcome by using shorter wavelength (higher frequency) lasers. The intensity of the Raman signals has a fourth power dependence on laser frequency ($I \alpha \upsilon^4 \alpha \lambda^{-4}$). The other way to increase the signal intensity is to tune or select a laser frequency closer to the absorption maximum of the compound under study. In this way the Raman intensity can be enhanced by 10^4 - 10^6 times under diluted conditions. Moreover, resonance effects selectively enhance the bands of the molecule, which are involved in the electronic transition close to the excitation wavelength.

Among the spectroscopic methods capable of addressing the 'vibronic' (*vide infra*) levels of metal complexes in uniquely revealing ways, resonance Raman (RR) spectroscopy stands out in regard to the range and depth of information that can be obtained. It is one of the techniques included in the present chapter, not only because of its inherent fundamental interest but on account of its versatility, frequently in tandem with other physical methods, such as UV/Vis absorption spectroscopy for probing molecular structure and reactivity. This has probably been most obviously felt in the field of bioinorganic chemistry where the body of data now available makes RR, and conventional Raman spectroscopy, together with ^{18}O isotope labelling, essentially a standard in the field.

Figure 2 shows the 'vibronic' energy level diagram used to illustrate the basic principles of Raman and resonance Raman spectroscopy. The term 'vibronic' here has its conventional meaning, referring to a vibrational transition coupled to an electronic transition and is particularly relevant in the context of RR spectroscopy. The very weak inelastic (Raman) scattering of monochromatic radiation (as little as 1 photon in 10^6-10^7), occurring via excitation to virtual levels (Figure 2), can be greatly enhanced when the excitation wavelength employed coincides with an electronic absorption (represented as $S_1 \leftarrow S_0$) in the scattering compound. This *resonantly enhanced* Raman (RR) scattering arises for those vibrational modes coupled to the electronic transition (hence the use of the term 'vibronic'), specifically those which undergo the greatest displacement in the excited state.

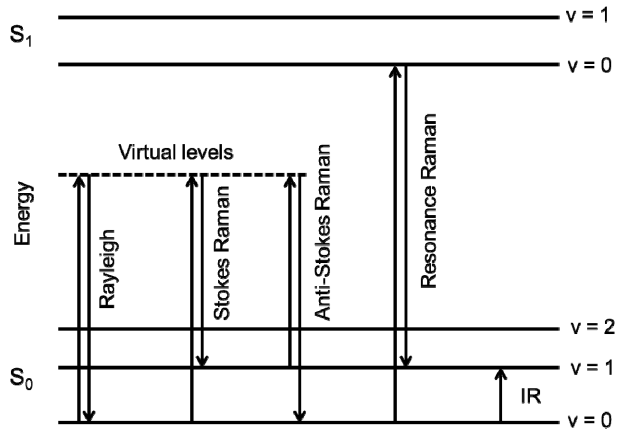

Figure 2 Representation of the processes that occur (from left to right) in non-resonant Rayleigh scattering, Stokes and anti-Stokes Raman resonance Raman spectroscopy and IR spectroscopy.

Raman and especially RR spectroscopy not only complement infrared and conventional UV/Vis absorption spectroscopy but are frequently uniquely informative in elucidating structural and dynamic behaviour of metal-centred species. For example, the RR spectra of $[(bpy)_2Ru^{II}(Mephpztr)]^{2+}$ in acetonitrile at various excitation wavelengths is shown in Figure 3.[2] Notably between λ_{exc} 355 nm and 473 nm the Raman spectrum is comprised of bands assignable exclusively to bpy based modes. At λ_{exc} 532 and 561 nm the spectrum is dominated by pyrazine based modes, which is confirmed by comparison with the spectra of $[([D_8]\text{-bpy})_2Ru^{II}(Mephpztr)]^{2+}$ and $[([H_8]\text{-bpy})_2Ru^{II}([D_3]\text{-Mephpztr})]^{2+}$. The wavelength dependence of the RR spectrum allows for assignment of the longest wavelength absorption band (at ca. 550 nm) to pyrazine based ^{1}MLCT ← GS transitions and the absorption band at ca. 430 nm to bpy based ^{1}MLCT ← GS transitions (Figure 3).

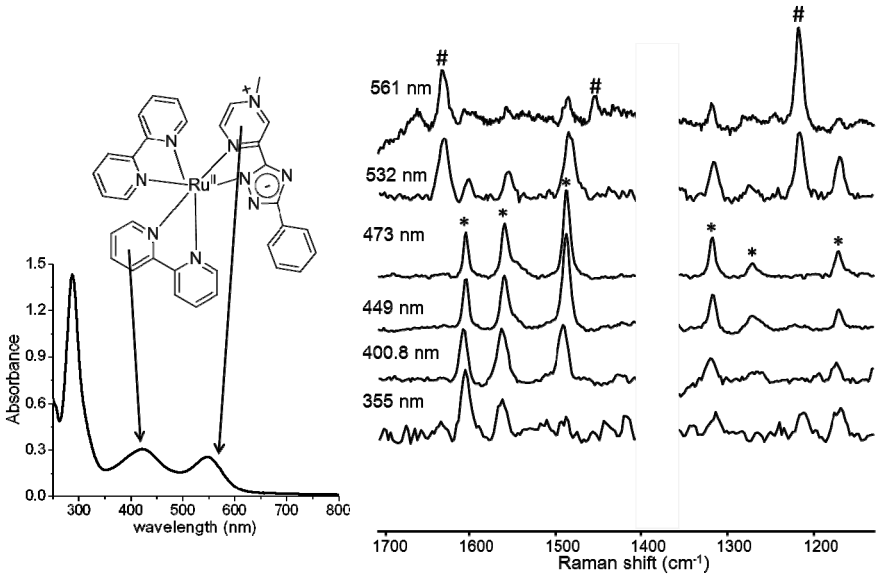

Figure 3 (left) structure and UV/Vis absorption spectrum of $[(bpy)_2Ru^{II}(Mephpztr)]^{2+}$ in acetonitrile and (right) wavelength dependent Raman spectra of $[(bpy)_2Ru^{II}(Mephpztr)]^{2+}$ in acetonitrile. Solvent bands are masked with a white box. * bands from bpy ligand and # bands from Mephpztr ligand.

I.1.3 Raman spectroscopy: fingerprinting active intermediates from metalloproteins to biomimetic oxidation catalysts

Metalloproteins perform an extensive range of chemical transformations, many of which have yet to be matched in function and selectivity in the synthetic laboratory. Mononuclear non-heme and heme iron and manganese proteins,[3] for example, carry out a diverse range of functions to achieve highly selective activation of C-H bonds in many organic substrates.[4] These catalytic capabilities are due to the remarkable properties of metal-containing active sites where both the first and second coordination sphere play important roles. Considerable experimental and theoretical effort has been directed towards mimicking and understanding so- called oxygen activated iron-containing proteins and already a wide range of such species, including oxo, hydroperoxo and peroxo species, have been prepared synthetically that serve as structural and spectroscopic models for proposed reactive intermediates in metalloproteins.[10-14]

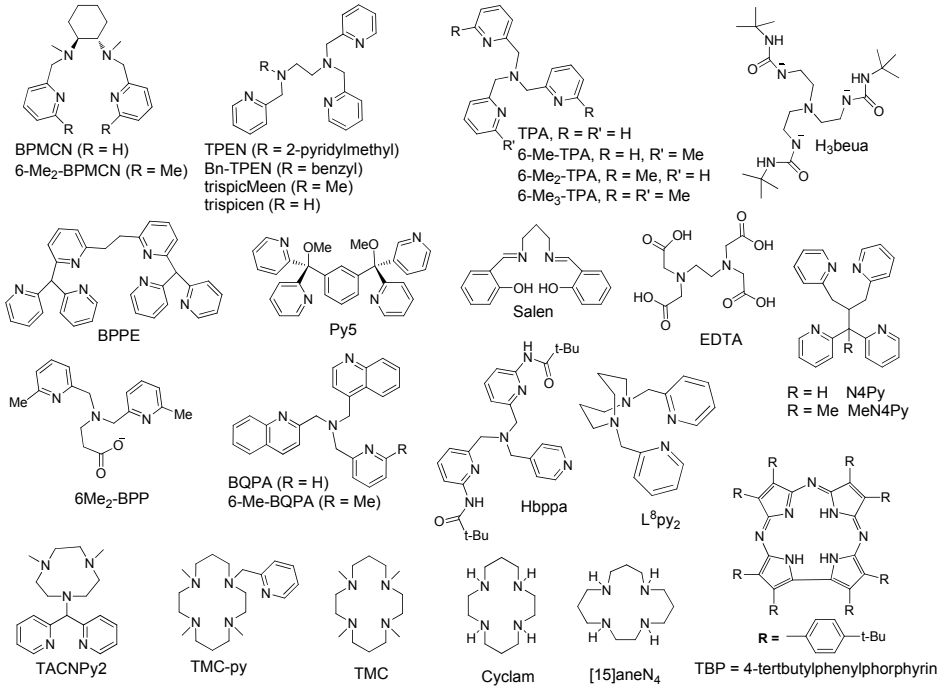

Figure 4 Structures of the ligands that are mentioned in this chapter.

These functional and structural mimics of active sites are important, not only from a biological perspective, but also for industrially critical applications, the oxidation of methane to methanol perhaps being among the most highly prized.[3,5] Raman and in particular RR spectroscopy have proven to be invaluable and versatile tools in this general area. The ability to obtain structural information regarding catalysts and enzymes present at relatively low concentration is one of the real strengths of the technique, where resonant enhancement of Raman scattering is possible. In the next few sections a number of recent examples are presented illustrative of the assignment of various important structures by means of Raman spectroscopy.

I.1.4 Characterisation of iron and manganese complexes by vibrational spectroscopy

The importance of mononuclear heme and non-heme iron based metalloenzymes ranging from cytochrome P450 to methane monooxygenase (MMO) and taurine catabolism dioxygenases (Tau-D), has stimulated considerable interest in synthetic high-valent iron-oxo species, which can serve as models for oxygen activated enzymes. In the case of non-heme iron based enzymes Que, Nam and co-workers and others have explored and isolated a considerable number of iron-oxo species and peroxo species over a wide range of oxidation states and spectroscopic data

from both UV/Vis absorption, FTIR and (resonance)Raman spectroscopy are now available (Chart I).[9-14] Characterising metal oxo and peroxo species especially those of Fe and Mn represents a considerable challenge due to their often very high reactivity. Overall the role played by vibrational and especially RR spectroscopy in the characterisation of non-heme iron and to a lesser extent manganese species can hardly be overestimated, providing not only evidence of structure but also detailed information regarding bond strengths.

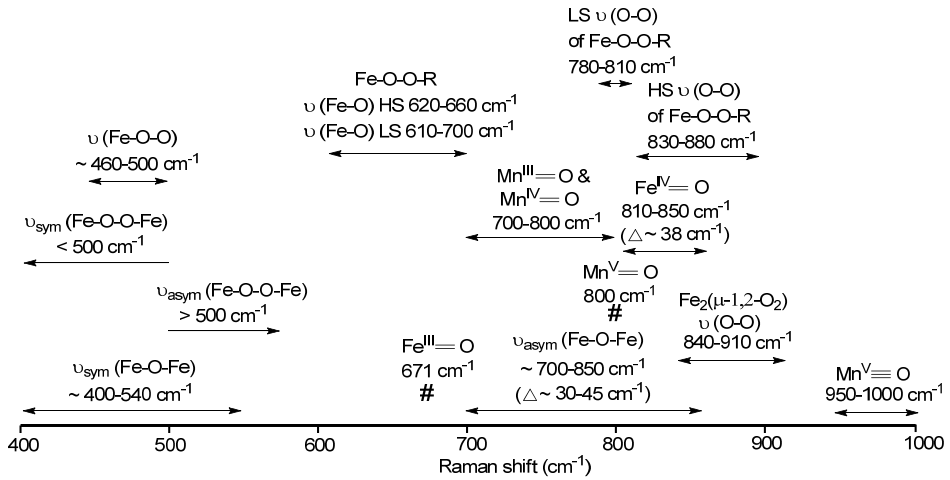

Chart 1 Wavenumber ranges in which O-O and M-O stretching vibrations are normally observed for various metal oxygen species (Δ indicates isotope ^{18}O shift).

In non-heme iron and manganese complexes a first indication of the structure of oxygen activated species can be garnered from their UV/Vis absorption spectra. In general iron and manganese complexes exhibit absorptions in the near-IR region (500-900 nm, see Chart 1), albeit with relatively low molar absorptivities. However, the absorption spectra cannot generally be used to discriminate between different possible structures (*e.g.*, Fe^{IV}=O *vs.* Fe^{III}-OO). It is at this level of assignment detail that RR spectroscopy is exceptionally useful, frequently alongside ^{18}O labelling to confirm band assignment (Chart 1).

I.1.5 Resonance Raman and the study of iron oxygen species

I.1.5.1 Iron(III)-hydroperoxo/alkyl peroxo (Fe^{III}-OOH(R)) species

From a biological perspective the bleomycin (BLM) family of antibiotics[6] that are used widely in chemotherapy, have stimulated considerable effort in understanding 'oxygen activated' iron complexes. In particular iron bleomycin reacts with oxygen to form the so-called 'purple' species, which exhibits an absorption band around 600 nm that is now known to be characteristic of the Fe^{III}-OOH species. In the case of Fe-BLM the active intermediate has been identified spectroscopically as a low-spin Fe^{III}-hydroperoxide.[7] Several structural mimics of the metastable purple Fe^{III}-OOH species have been prepared, in particular complexes with neutral pentadentate ligands *e.g.*, 1,1-di(pyridin-2-yl)-N,N-bis(pyridin-2-ylmethyl)ethanamine (N4Py) *etc*.[8] Resonance Raman spectroscopy has proven itself to be invaluable in gaining detailed insight into the properties of the low-spin Fe^{III}-OOH moiety and of the related Fe-OO^- (side-on bound peroxy species), formed upon deprotonation.[9,10a] Formation of the corresponding conjugate bases was confirmed by the red shift in the complexes absorption maxima and by electrospray mass spectrometry.

Table 1 UV/Vis absorption and resonance Raman signatures on selected Fe^{III}-OO(H/R) species.

Fe^{III}-OOR (R = H or ^{t}Bu)	λ_{max} (nm) (ε, M^{-1} cm^{-1})	O-O (^{18}O-^{18}O) cm^{-1}	Fe-O (Fe-^{18}O) cm^{-1}	Experimental conditions
[10a][(TACNPy2)Fe^{III}(OOH)]$^{2+}$ (LS)	520	781	639	In acetone, at λ_{exc} 568.2 nm, at 77 K
[10b][Fe^{III}(TPA)(OO^{t}Bu)(acetone)]$^{2+}$ (LS)	560 (900)	788	693	In acetone, at λ_{exc} 568.2 nm, 77 K
[10c,d][Fe^{III}(β-BPMCN)(OO^{t}Bu)(X)]$^{2+}$ (LS)	566 (2500)	789	680	In DCM, at λ_{exc} 647.1, 568.2, 488 nm, at 77 K
[10b][Fe^{III}(5-Me_3-TPA)(OO^{t}Bu) (acetone)]$^{2+}$ (LS)	560 (1500)	789	691	In d_6-acetone, at λ_{exc} 568.2 nm, at 77 K
[9][(TPA)Fe^{III}(OOH)]$^{2+}$	538	789	626	In THF/CD_3CN (1:4), at λ_{exc} 568.2 nm, at 223 K
[9,10a][(N4Py)Fe^{III}(OOH)]$^{2+}$ (LS)	548 (1300)	790 (-44)	632 (-16)	In acetone, at λ_{exc} 568.2 nm, at 77 K
[10f][(6-MeTPA)Fe^{III}(OO^{t}Bu) (H_2O)]$^{2+}$ (LS) [(6-MeTPA)Fe^{III}(OO^{t}Bu)(H_2O)]$^{2+}$ (HS)	598	790 842, 878	682 648	In CH_3CN, at λ_{exc} 599.5 nm, at 77 K
[10a][(5-(MeO)-N4Py)Fe^{III}(OOH)]$^{2+}$ (LS)	549 (1030)	791	644	In acetone, at λ_{exc} 568.2 nm, at 77 K
[10a,c][(β-BPMCN)Fe^{III}(OO^{t}Bu)(X)]$^{2+}$ (LS)	600 (2500)	793	685	In CH_3CN, at λ_{exc} 647.1 nm, at 77 K
[10a][(5-Br_2-N4Py)Fe^{III}(OOH)]$^{2+}$ (LS)	557 (1210)	795	641	In acetone, at λ_{exc} 568.2 nm, at 77 K

[10e][(TPA)Fe^{III}(OO^tBu)(H_2O)]$^{2+}$ (LS)	600	796	696	In CH_3CN, at λ_{exc} 599.5 nm, at 77 K
[10f][(TPEN)Fe^{III}(OOH)]$^{2+}$ (LS)	541	796	617	In CH_3OH, at λ_{exc} 568 nm, at ambient temperature
[10f,g][(trispicMeen)Fe^{III}(OOH)]$^{2+}$ (LS)	537 (1000)	796 (-45)	617 (-17)	In CH_3OH, at λ_{exc} 568 nm (25 mW), at ambient temperature
[10f][(trispicen)Fe^{III}(OOH)]$^{2+}$ (LS)	531 (950)	796 (-50.5)	625 (-23)	In CH_3OH, at λ_{exc} 568 nm, at ambient temperature
[10h][([15]aneN_4)Fe^{III}(OO^tBu) (SC_6H_5-p-SC_6F_5)]$^+$ (LS)	508	799 (-34)	623 (-26)	In DCM, at λ_{exc} 514 nm, at 110 K
[10i][([15]aneN_4)Fe^{III}(OO^tBu)(SC_6H_5)]$^+$ (LS)	526	803 (-35)	611 (-27)	In DCM, at λ_{exc} 514 nm, at 110 K
[10h][([15]aneN_4)Fe^{III}(OO^tBu) (SC_6H_5-p-Cl)]$^+$ (LS)	524	803 (-35)	612 (-27)	In DCM, at λ_{exc} 514 nm, at 110 K
[10a][(Py5)Fe^{III}(OOH)]$^{2+}$ (LS)	592	806	627	In acetone, at λ_{exc} 568.2 nm, at 77 K
[10i][(bpy)$_2$$Fe^{III}$($OO^tBu$) (BzOH)]$^{2+}$ (LS)	640	808	678	In CH_3CN, at λ_{exc} 628 nm, at 77 K
[10j][(H_2bppa)Fe^{III}(OOH)]$^{2+}$ (HS)	568 (1200)	830 (-17)	621 (-22)	In d_6-acetone, at λ_{exc} 570 nm, at 223 K
[10k][(L^8py$_2$)Fe^{III}(OO^tBu)(OTf)]$^+$ (HS)	580	833, 870	627	In DCM, at λ_{exc} 514.5 nm, at 77K
[10k][(L^8py$_2$)Fe^{III}(OO^tBu)(OBz)]$^+$ (HS)	545	832, 873	623	In DCM, at λ_{exc} 514.5 nm, at 77K
[10k][(L^8py$_2$)Fe^{III}(OO^tBu)(OTf)]$^+$ (HS)	550	831, 878	623	In DCM, at λ_{exc} 514.5 nm, at 77K
[10e][(6-Me_3TPA)Fe^{III}(OO^tBu) (H_2O)]$^{2+}$ (HS)	562	842, 877	637	In CH_3CN, at λ_{exc} 599.5 nm, at 77 K
[10e][(6-Me_2TPA)Fe^{III} (OO^tBu) (H_2O)]$^{2+}$ (HS)	552	842, 878	648	In CH_3CN, at λ_{exc} 599.5 nm, at 77 K
[10l][(6-Me_3TPA)Fe^{III} (OO^tBu)(OBz)]$^+$ (HS)	514	844, 880	648	In DCM, at λ_{exc} 514.5 nm, at 80 K
[11a][(TMC)Fe^{III}(OOH)]$^{2+}$ (HS)	526	855, 868 (-48)	658 (-25)	In d_6-acetone, at λ_{exc} 531 nm, at 77 K

Where HS is high spin and LS is low spin

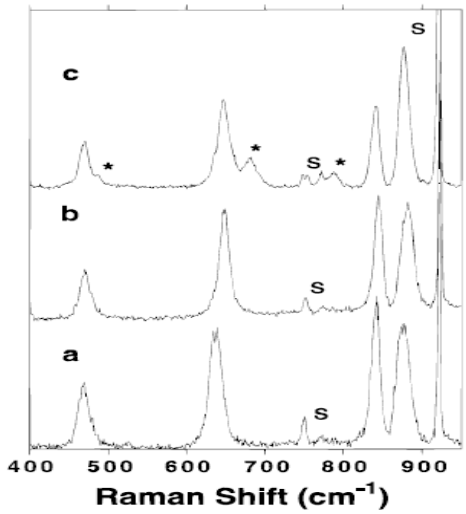

Figure 5 Resonance Raman spectra of intermediates obtained with 514.5 nm excitation on frozen CH_3CN solutions: (a) $[(6\text{-}Me_3TPA)Fe^{III}(OO^tBu)(H_2O)]^{2+}$, (b) $[(6\text{-}Me_2TPA)Fe^{III}(OO^tBu)(H_2O)]^{2+}$, (c) $[(6\text{-}MeTPA)Fe^{III}(OO^tBu)(H_2O)]^{2+}$ (from tBuOOH; peaks marked with an asterisk are from the low-spin isomer). Solvent bands are labelled "s". Reproduced from Reference 10e with permission from American Chemical Society (**1997**).

In recent years characteristic vibrational bands for these intermediates have been determined from their resonance Raman spectra, primarily by virtue of the characteristic LMCT transitions of, *e.g.*, Fe^{III}-OOR species that absorb in the range 500 to 600 nm. UV/Vis absorption and resonance Raman signatures on selected Fe^{III}-OOH(R) are given in Table 1. Indeed the ν(O-O) stretching mode is now informative of the spin state of such species; low-spin Fe^{III}-OOR complexes typically exhibit weak ν(O-O) bands in the range 780-810 cm^{-1} compared to their high spin analogues which have vibrational features in the range 830-880 cm^{-1}. Fe-O stretching frequency in these complexes typically falls between 610-700 cm^{-1} and does not show similar correlations with spin state except that it has been suggested that the low-spin Fe^{III}-OOR complexes exhibit relatively intense Fe-O bands, compared to high-spin Fe^{III}-OOR complexes. It should be noted that that there is no apparent correlation between high and low spin complexes and the Fe-O stretching frequency (Table 1). The value of RR spectroscopy in assignment of spin states in solution is further exemplified in the complex $[(6\text{-}MeTPA)Fe^{III}(OO^tBu)(H_2O)]^{2+}$ (where 6-MeTPA is tris(2-(6-methyl)pyridylmethyl)amine). This complex exhibits EPR signals at $g = 4.3$ and at $g = 2$, *i.e.* both high and low spin states, respectively, which was manifested in the resonance Raman spectra as a mixture of high-spin and low-spin Fe^{III}-OOR features (Figure 5).[10e]

I.1.5.2 Iron(III)-peroxo (Fe^{III}-OO) species

Iron(III)-peroxo complexes absorb at longer wavelengths compared to their hydro/alkyl peroxo analogues. These complexes show the characteristic O-O stretching band in the range 800-830 cm^{-1}, as with high spin Fe^{III}-OOH complexes (Table 2). This makes it particularly difficult to identify the iron(III) peroxo with hydro/alkyl peroxo complexes. However, the Fe-O band is distinctly different in these two species. In contrast to iron(III)-hydro/alkyl peroxo complexes, the stretching mode of Fe-O band in iron(III)-peroxo complexes was observed between 460-500 cm^{-1}. This band is far lower in energy than the corresponding Fe-O stretching frequency in iron(III)-hydroperoxo complexes (610-700 cm^{-1}). For example, high-spin $[(TMC)Fe^{III}(OOH)]^{2+}$ complex shows a O-O stretching mode at 861 cm^{-1}, which is 34 cm^{-1} higher than the corresponding conjugate base $[(TMC)Fe^{III}(OO)]^{+}$. This indicates a weakened O–O peroxo bond, which is ascribed to back bonding from iron to the peroxo antibonding π^* orbital, which considerably weakens the O–O bond. UV/Vis absorption and Raman frequencies of known Fe^{III}-OO species are summarised in Table 2.

The contribution of resonance Raman spectroscopy, as one of an array of techniques, in helping to unravel important issues in catalysis and especially in oxidation catalysis is exemplified in the recent reports by Nam and co-workers[11] on the isolation of three oxygen activated iron intermediates implicated in various catalytic cycles; namely $[(TMC)Fe^{III}(OO)]^{+}$ (**1**), $[(TMC)Fe^{III}(OOH)]^{2+}$ (**2**) and $[(TMC)Fe^{IV}(O)]^{2+}$ (**3**) where TMC is the macrocyclic ligand 1,4,8,11-tetramethyl-1,4,8,11-tetraazacyclotetradecane. Despite their intrinsic instability, crystal structures of two of these species, **1** and **3**, are available. Further essential structural information about these active intermediates is deduced from UV/Vis absorption and Raman spectroscopy, as Figure 6 shows.

Table 2 UV/Vis absorption and RR signatures on selected Fe^{III}-OO species.

Complex / Fe^{III}-OO	λ_{max} (nm) (ε, M^{-1} cm^{-1})	O-O (^{18}O-^{18}O) cm^{-1}	Fe-O (Fe-^{18}O) cm^{-1}	Experimental conditions
[12a][(OEP)Fe^{III}(OO)]$^-$ (heme)	545, 573 (584 sh)	805 (-46) 780 (-49)	Not mentioned	Me_2SO/18-crown-6, at RT (IR) at λ_{exc} 528.7 nm, frozen sample at 170 K (RR)
[12b][(EDTA)Fe^{III}(OO)]$^{3-}$ (HS)	520	816 (-40)	459 (-13)	In water, at λ_{exc} 514.5 nm (100 mW), at 70 K
[10g][(TPEN)Fe^{III}(OO)]$^+$ (HS)	755	817	470	In MeOH, at λ_{exc} 647 nm, ambient temperature
[10g][(trispicMeen)Fe^{III}(OO)]$^+$ (HS)	740 (500)	819	470	In MeOH, at λ_{exc} 647 nm, ambient temperature
[11a][(TMC)Fe^{III}(OO)]$^+$	782	825(-44)	487 (-19)	In d_6-acetone, at λ_{exc} 785 nm (300 mW), at 77 K
[10a][(N4Py)Fe^{III}(OO)]$^+$ (HS)	685(520)	827(-47)	495 (-17)	In MeOH, at λ_{exc} 647 nm, at 77 K

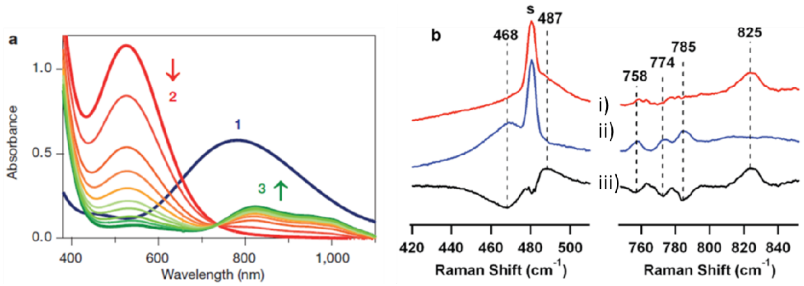

Figure 6 (a) UV/Vis absorption spectra of **1**, **2** and **3**; arrows indicate spectral changes for the conversion of **2** to **3** in the reaction of **1** (1 mM) and 3 equiv. $HClO_4$ in acetone/CF_3CH_2OH (3:1) at -40 °C and (b) RR spectra of **1** in d_6-acetone with ^{16}O (i) and ^{18}O (ii) isotopic substitution in the region of Fe-O and O-O stretches. (iii) is the ^{16}O and ^{18}O difference spectrum. The band marked with "s" is assigned to the solvent. Reproduced from Reference 11b with permission from Nature (**2012**).

The resonantly enhanced vibrational stretching modes for the O-O bond at 825 and 861 cm^{-1} (latter band is not shown in Figure 6) for **1** and **2**, respectively, confirmed their high spin electronic state (by comparison with literature precedents, see Chart 1). The decrease in the bond strength from the peroxo to the hydroperoxo reflects the increased back bonding from Fe(III) into the peroxo antibonding orbitals. The Fe-O band was observed at 487 cm^{-1} for **1** and at 658 cm^{-1} for **2**. In the case of **3**, the Fe^{IV}=O band was observed at 834 cm^{-1}, and shifted by 34 cm^{-1} upon ^{18}O labelling, as expected for an Fe-O bond. These data demonstrate that the extent

to which species can be characterised even in circumstances of relatively high instability.

I.1.5.3 Metal-oxo ($M^{III/IV/V}$=O) species

High-valent iron-oxo species have commonly been considered as intermediates in the reaction of non-heme iron enzymes with dioxygen. High valent non-heme Fe^{IV}=O complexes exhibit near-IR transitions with relatively low molar absorptivity. Their lower molar absorptivities suggest that these electronic transitions are not charge-transfer transitions but more likely ligand field in origin. In non-heme iron complexes the Fe^{IV}=O stretch was normally observed in the range between 810-850 cm^{-1} (Table 3). The modes were assigned definitively by incorporating ^{18}O into the oxo complex. The Fe^{IV}=O band shifts to lower wavenumber shift by 38 cm^{-1} when ^{18}O is substituted for ^{16}O. Additionally the band position is markedly influenced by the axial ligands. Notably, the ν(Fe=O) modes of $[(TMC)Fe^{IV}(O)(NCS)]^+$ and $[(TMC)Fe^{IV}(O)(N_3)]^+$ are at lower frequency relative to that of $[(TMC)Fe^{IV}(O)(CH_3CN)]^{2+}$, which reflects the substitution of the π-acidic CH_3CN with the more π-basic N_3^- and NCS^- ligands, yielding ν(Fe=O) frequencies closer to that observed for the TauD intermediate (821 cm^{-1}).[14f] The Fe^{III}=O vibration[14a,b] at 671 cm^{-1} for $[(H_3beua)Fe^{III}(O)]^{2-}$ occurs outside the range reported for heme and non-heme Fe^{IV}=O systems; for instance, a ν(Fe-O) at 834 cm^{-1} was found for the monomeric Fe^{IV}=O complex $[(TMCPy)Fe^{IV}(O)(CH_3CN)]^{2+}$.[14h]

Recently, Que reported the existence and spectroscopic characterisation of a $[(TAML)Fe^{V}(O)]^-$ species.[13] The Fe^{V}=O band was observed at 798 cm^{-1} along with an associated 1587 cm^{-1} overtone. The corresponding conjugate acid shows the band at 811 cm^{-1} along with an overtone at 1613 cm^{-1}. These vibrational frequencies at 798 and 811 cm^{-1} are at the lower end of the reported Fe^{IV}=O vibrational frequencies. Resonance Raman spectroscopy has proven useful to identify other metal oxo intermediates also. In the case of Ru complexes, the Ru^{IV}=O band occurs at ~800 cm^{-1}, which is lower compared to Fe^{IV}=O species. The Ru^{IV}=O band shifts to lower frequency by 40 cm^{-1} when ^{18}O is substituted for ^{16}O.

Table 3 UV/Vis absorption and Resonance Raman signatures on selected metal oxo species.

Metal oxo	λ_{max} (nm) (ε, M^{-1} cm^{-1})	M-O (M-^{18}O) (cm^{-1})	Experimental conditions
[14a,b][$(H_3buea)Fe^{III}(O)]^{2-}$	---	671 (-26)	FTIR solid
[14c][$(H_3buea)Mn^{III}(O)]^{2-}$	---	700 (-28)	FTIR solid
[14d][$(BQCN)Mn^{IV}(O)]^{2+}$	630 (400)	707 (-31)	In 9:1 acetone/water at 409 nm, at 233 K
[14e]$HO\text{-}Mn^{V}$=O (Heme)	---	791 (-34) (Mn^{V}=O) 518 (-27) (Mn^{V}-OH)	In CH_2Cl_2/CH_3CN at 413.1 nm, at 278 K
[10d][$(TPAH^{+})Ru^{IV}(O)(bpm)]^{3+}$	690	800 (-43)	In water at 363.8 nm, at 295 K
[14f][$(TPA)Ru^{IV}(O)(H_2O)]^{2+}$	465	806 (-42)	In water at 442 nm
[13][$(TMC)Fe^{V}(O)(NC(O)CH_3)]^{+}$	410 (4000), 780 (430)	798 (-35) 1587 (overtone)	In CH_3CN at 413 nm , at 77 K
[14f][$(TMC)Fe^{IV}(O)(N_3^{-})]^{+}$	805, 1050	812 (-33)	In CH_3CN at 406.4 nm, at 295 K
[14g][$(TPEN)Fe^{IV}(O)]^{2+}$	730 (380)	818 (-24)	FTIR, In CH_3CN at 298 K
[14f][$(TMC)Fe^{IV}(O)(NCS)]^{+}$	850, 1010	820 (-34)	In CH_3CN at 406.4 nm, 293 K
[14h][$(TMC\text{-}Py)Fe^{IV}(O)]^{2+}$	834	826 (-34)	In CH_3CN at 407 nm, frozen solution
[14f][$(TMC)Fe^{IV}(O)(CH_3CN)]^{2+}$	820	834 (-34)	In CH_3CN at 406.4 nm, 293 K
[14i][$(N4Py)Fe^{IV}(O)]^{2+}$	695	840 (-34)	In 1:3 water/CH_3CN at 407 nm, at 273 K
[14i][$(MeN4Py)Fe^{IV}(O)]^{2+}$	687	843 (-36)	In water and in CH_3CN at 473 nm and 785 nm, at RT
[14j][$(TBC)Fe^{IV}(O)(CH_3CN)]^{2+}$	885	842 (-38)	In CH_3CN at 442 nm, 293 K
[14k][$(salen)Fe^{IV}(O)$]	---	851 (-35)	At 406.7 nm, 15 K, O_2 matrix
[14b]$(TTPPC)Mn^{V}$≡O (heme)	---	952 (-39)	1.0 mM CH_2Cl_2 at 413.1 nm
[14l]Mn^{V}≡O	---	979 (-37)	FTIR solid
[14l]$(TBP)_8(Cz)\,Mn^{V}$≡O $(TBP)_8(Cz)\,Mn^{V}$≡O	418, 634 ---	979 (-41) 997 (-43)	In CH_2Cl_2 at 413.1 nm (RT) KCl pellet at 413.1 nm (RT)

Interestingly, reported non-heme Mn^{III}=O[14c] and Mn^{IV}=O[14d] complexes show characteristic Mn-O stretching bands at ~700 cm^{-1}. In the former case the measurement was obtained on a solid sample by FTIR and the complex has trigonal bipyramidal geometry. $[(BQCN)Mn^{IV}(O)]^{2+}$ is an octahedral complex and the Raman spectrum was obtained in acetone/water. One other point to emphasis here is that the Mn^{III}=O species has three intra-molecular hydrogen bonds in the solid state. The Mn^{IV}=O stretch in the $[(BQCN)Mn^{IV}(O)]^{2+}$ complex is much lower in frequency compared to the corresponding Mn^{III}=O species. The complex

$[(H_3buea)Mn^{IV}(O)]^-$ exhibits a band at $\nu_{Mn=O}$ = 737 cm^{-1}, which is closer to the Mn^{IV}=O porphyrin complexes ($\nu_{Mn=O}$ ~ 750 cm^{-1}).[14c,d]

Other intermediates such as Mn^V=O and Mn^V≡O, can be easily distinguished using Raman spectroscopy.[14e,l] The former shows a band at ~800 cm^{-1} but the latter shows a band in the range 950-1000 cm^{-1}. In the case of (TTPPC)Mn^V≡O a very strong band was observed at 952 cm^{-1}, which was shifted to 913 cm^{-1} upon ^{18}O substitution assigning it as a Mn-O stretching band. However, the observed value of 952 cm^{-1} is significantly higher than the doubly bonded Mn^{III}=O (700 cm^{-1}), Mn^{IV}=O (700 cm^{-1}), porphyrinic HO-Mn^V=O (791 cm^{-1})[14e] and O=Mn^V=O ($\nu_{Mn=O}$ = 741-743 cm^{-1})[15] complexes. Moreover, the calculated force constant for the 952 cm^{-1} mode is 6.61 mdyn/Å, which is consistent with assignment of the mode as Mn^V≡O.

I.1.5.4 Diiron (Fe^{III}-O-O-Fe^{III}) complexes

(Resonance)Raman spectroscopy is also employed to probe the structure of the $Fe_2(\mu$-1,2-$O_2)$ core. The vibrations of the Fe-O-O-Fe unit consist of three modes: the O-O stretch, symmetric and asymmetric *ν*(Fe-O-O-Fe) deformations. The O-O stretching frequency is observed in the range 840-910 cm^{-1}. This band is easily confused with the O-O stretching frequencies of other intermediates such as Fe^{III}-OOR and Fe^{III}-OO. But one can use the Fe-O-O-Fe symmetric and asymmetric modes as marker bands, as they are not observed in the other intermediates. The ν_{sym}(Fe-O-O-Fe) mode is typically found below 500 cm^{-1} (Table 4). On the other hand, the ν_{asym}(Fe-O-O-Fe) mode is found above 500 cm^{-1}.

Table 4 UV/Vis absorption and Resonance Raman signatures on selected Fe^{III}-O-O-Fe^{III} species.

Fe^{III}-O-O-Fe^{III}	λ_{max} (nm) (ε, M^{-1} cm^{-1})	O-O ν_{sym} (^{18}O-^{18}O) cm^{-1}	Fe-O-O-Fe ν_{sym} (Fe-^{18}O-^{18}O-Fe) cm^{-1}	Experimental conditions
[16a][Fe^{III}_2(μ-O)(μ-1,2-O_2)(6-Me_3-TPA)$_2$]$^{2+}$	648(1200) 846 (230)	848 (-46) FD	462 (-21) FD	At 628 nm, in CH_3CN
[16b][Fe^{III}_2(μ-O)(μ-1,2-O_2)(BQPA)$_2$]$^{2+}$	620 (1000)	844 (-44)	464 (-17)	At 647.1 nm, in CH_3CN on gold plated copper cold finger
[16c][Fe^{III}_2(μ-O)(μ-1,2-O_2)(6-Me_2BPP)$_2$]$^{2+}$	577 (1500)	847 (-33)	465 (-19)	At 600 and 580 nm (30 mW), in MeOH at 193 K
[16b][Fe^{III}_2(μ-O)(μ-1,2-O_2)(6-Me_3-BQPA)$_2$]$^{2+}$	Not reported	847 (-44)	463 (-21)	At 647.1 nm, in CH_3CN on gold plated copper cold finger
[16b][Fe^{III}_2(μ-O)(μ-1,2-O_2)(6-Me-BQPA)$_2$]$^{2+}$	Not reported	853 (-45)	463 (-15)	At 647.1 nm, in CH_3CN on gold plated copper cold finger
[16d][Fe^{III}_2(μ-1,2-O_2)(μ-O_2CPh)$_2$(Tp^{ipr2})$_2$]	682 (2500)	876 (-49)	418 (-9)	At 676 nm (20 mW), in toluene at 193 K
[16e][Fe^{III}_2(μ-1,2-O_2)(μ-$_2$$CCH_2Ph$)$_2$($Tp^{ipr2}$)$_2$]	694 (2650)	888 (-46)	415 (-11)	At 647 nm (50 mW), in toluene at 195 K
[16b][Fe^{III}_2(μ-1,2-O_2)(N-Et-PTB)($OPPh_3$)$_2$]$^{2+}$	588 (1500)	900 (-50)	471 (-16)	At 647.1 nm, in CH_3CN on gold plated copper cold finger
[16c][Fe^{III}_2(μ-OH)(μ-1,2-O_2)(6-Me_2BPP)$_2$]$^{2+}$	644 (3000)	908 (-47) FD	465 (-11) FD	At 600 and 580 nm (30 mW), in MeOH at 193 K

Where FD is Fermi doublet

I.1.5.5 μ-oxo iron(III) dimers (Fe^{III}-O-Fe^{III})

The Raman and infrared spectral properties of μ-oxo and μ-hydroxo diiron(III) complexes are well documented in Reference 17. In many cases ν_{sym}(Fe-O-Fe) and ν_{asym}(Fe-O-Fe) have been identified definitively by their ^{18}O isotope shifts. The energies of the two Fe-O-Fe vibrations show the expected dependence on Fe-O-Fe angle. As the Fe-O-Fe angle decreases the frequency of the asymmetric stretch decreases while the frequency of the symmetric stretch increases. These data indicate that knowledge of ν_{sym} and ν_{asym} should allow the prediction of an Fe-O-Fe angle within 10° of the correct value. A survey of known (μ-oxo)diiron(III) complexes reveals that the asymmetric Fe-O-Fe stretch occurs between ~700-850 cm^{-1} and symmetric Fe-O-Fe stretch occurs between ~400-540 cm^{-1}. The asymmetric stretch shifts to lower energy by ~30-45 cm^{-1} when ^{16}O is substituted for ^{18}O.[17]

I.1.6 Second coordination sphere interactions in molecular systems

A recent example relevant to catalytic water oxidation, concerns the Keggin-type complexes $[Ru^{III}(H_2O)SiW_{11}O_{39}]^{5-}$ and $[Ru^{III}(H_2O)GeW_{11}O_{39}]^{5-}$ employed as catalysts for water oxidation to dioxygen using Ce(IV) as a one electron oxidant (it should be noted that water oxidation is, overall, a four electron process). Cyclic voltammetry indicated that a Ru(III)-OH species could undergo oxidation to a Ru(V)-oxo species and indeed such a species was identified by UV/Vis absorption, resonance Raman and EPR spectroscopy. Of note with regard to the present discussion is the use of $H_2{}^{18}O$ labelling. The Ru(V)=O stretching mode was identified at 800 cm^{-1},[18] however, the isotopic shift was only 15 cm^{-1} rather than the expected 40 cm^{-1}, based upon a simple Hooke's law two-atom harmonic oscillator approximation. The authors considered this to indicate that Ce(IV) was binding to the oxygen atom, hence rendering the two atom oscillator approximation for predicting the $^{16/18}O$ shift an oversimplification but highlighting the role of second coordination sphere type interactions in determining the behaviour of such systems.

The effect of hydrogen bonding on Fe^{III}=O and Mn^{III}=O bond strengths has implications for the mechanism by which the oxygen evolving complex of photosystem II operates.[19] The issue has been explored recently[19] in some elegantly designed systems to investigate the effects of hydrogen bonding on the reactivity and spectral properties of M=O species. The ligand system shown in Figure 4 enforces penta-coordination on the metal centre and holds hydrogen bond donor units in proximity to the oxygen of the M=O unit. The strength of the hydrogen bond donors can be tuned systematically.

A further challenge in designing these systems (see Figure 7) was to overcome the strong tendency for metal ions to form M-O-M bonds. The complexes $[(H_3buea)M^{III}(O)]^{2-}$ in Figure 7, where M = Fe or Mn and H_3buea = tris[(*N*'-tert-butylureaylato)-*N*-ethylene]aminato), were formed by direct activation of dioxygen.[20] In these systems isotopic labelling studies as well as the assignment of bands in the resonance Raman spectra of the complexes confirmed that the oxygen source for the oxo ligand was dioxygen; the ν(Fe-O) feature at 671 cm^{-1} shifted to 645 cm^{-1} with $^{18}O_2$ and similarly the ν(Mn-O) band at 700 cm^{-1} shifted to 672 cm^{-1}. However, demonstrating the occurrence of hydrogen bonding interactions between the M=O unit and the proximal amide N-H groups is not straightforward. In the present instance the weakening of the M-O bond as a result of H-bond interactions

was easily apparent from the Raman shift of the respective ν(M-O) mode.

Oxidation of the $[(H_3buea)Mn^{III}(O)]^{2-}$ complex to the Mn^{IV}=O state and subsequently to the Mn^{V}=O state was achieved electrochemically at low temperature and resonance Raman proved to be an important tool in characterising the details of the system.[21]

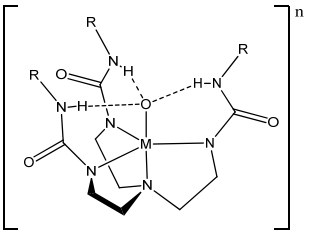

Figure 7 The H_3buea ligand (where R = tBu) developed by Borovik and co-workers to probe second coordination sphere effects (*i.e.* hydrogen bonding interactions) in a synthetic system. The cavity provides up to three H-bonding opportunities and the bulky R groups preclude formation of oxo bridged dinuclear complexes.[20]

These studies reflect the increasing emphasis placed on understanding the second coordination sphere on the activity and properties on metal complexes, in particular metal-oxo and metal-peroxy species, as proposed by Alfred Werner over a century ago.[22]

I.2 Electrochemical properties of Fe^{IV}=O complexes

Knowledge of the electrochemical properties of Fe^{IV}=O complexes is desirable to understand their role in the oxidation of organic substrates.[23] Unfortunately, data on the Fe^{IV}/Fe^{III} redox couple of non-heme iron complexes remains equivocal in literature primarily due to the sluggish rates of heterogeneous electron transfer which limit the utility of cyclic voltammetry.[24] The available electrochemical data on non-heme Fe^{IV}=O and the corresponding Fe(II) complexes in water and in acetonitrile is summarized in Table 5.

$[(N4Py)Fe^{IV}(O)]^{2+}$ is perhaps the most studied of the non-heme Fe^{IV}=O complexes. $[(N4Py)Fe^{II}(CH_3CN)]^{2+}$ itself shows a reversible redox wave at +1.01 V *vs.* SCE in anhydrous acetonitrile, which is assigned to the $Fe^{III}/Fe^{II}(CH_3CN)$ redox couple.[23,25] As shown in chapter 2, in water this complex shows a reversible redox wave at +0.4 V *vs.* SCE ($Fe^{III}/Fe^{II}(H_2O/OH)$) depending on the pH of the solution due to the exchange of CH_3CN with an aqua/hydroxide ligand upon dissolution.[25] In contrast to $[(N4Py)Fe^{II}(CH_3CN)]^{2+}$, $[(N4Py)Fe^{IV}(O)]^{2+}$ reported by Que and co-workers to show an irreversible reduction wave in its cyclic voltammogram at -0.13 V *vs.* SCE in anhydrous acetonitrile, which was ascribed to the $Fe^{IV}/Fe^{III}(O)$ redox couple.[23]

The question arises though as to why the $Fe^{IV}/Fe^{III}(O)$ reduction occurs at a much lower potential than its $Fe^{III}/Fe^{II}(CH_3CN)$ or $Fe^{III}/Fe^{II}(OH)$ redox couple? A simple answer is that the reduction of Fe^{IV}=O to Fe^{III}-OH is proton coupled and, hence, in anhydrous acetonitrile reduction becomes more difficult in the absence of protons. However, this would make it a very weak oxidant. Regardless the stability of the Fe^{IV}=O complexes, means that it is possible to generate the Fe^{IV}=O species in acetonitrile and in DCM in the presence water.[26] Using spectropotentiometric titrations Que and co-workers determined the oxidation potential for the $Fe^{IV}/Fe^{III}(O)$ couple in acetonitrile containing water to be +1.3 *vs.* SCE, in sharp contrast to their initial report and inconsistent with the proton coupled nature of the process (the potential gap is too large, *i.e.* +1.43 V).[26] However, a reversible redox wave for $Fe^{IV}/Fe^{III}(O)$ in water at +0.41 V *vs.* SCE was reported by same group.[27] Surprisingly, the corresponding $Fe^{III}/Fe^{II}(OH)$ redox couple, which shows a reversible redox wave in the same potential region was not considered in their interpretation of the cyclic voltammograms. The authors claimed that the irreversibility in acetonitrile is due to slow electron transfer rates. If this were the case why would the same complex show a reversible redox wave in water?

Furthermore for the same complex Nam and Fukuzumi proposed a reduction potential of +0.51 V *vs.* SCE in acetonitrile for the Fe^{IV}/Fe^{III}(O) couple based on spectrophotometric redox titrations.[28] The reduction potentials of +0.49 V for $[(BnTPEN)Fe^{IV}(O)]^{2+}$, +0.39 V for $[(TMC)Fe^{IV}(O)(CH_3CN)]^{2+}$, +0.13 V for $[(TMC)Fe^{IV}(O)\{OC(O)CF_3\}]^{+}$ and -0.05 V for $[(TMC)Fe^{IV}(O)(N_3)]^{+}$ *vs.* SCE, were also reported by applying same method.[28]

Table 5 Reported redox potentials of known Fe^{IV}=O complexes.

Complexes	Fe^{III}/Fe^{II} in anhydrous CH_3CN[a,b]	Fe^{III}/Fe^{II} in H_2O[a,c]	Fe^{IV}/Fe^{III} (ox) in anhydrous CH_3CN[b]	Fe^{IV}/Fe^{III} (red) in anhydrous CH_3CN[b,d]	Fe^{IV}/Fe^{III} (red) in CH_3CN[e]	Fe^{IV}/Fe^{III} (ox) in H_2O[f]
$[(N4Py)Fe^{IV}(O)]^{2+}$	+1.01	+0.4	+1.30	-0.13	+0.51	+0.41
$[(BnTPEN)Fe^{IV}(O)]^{2+}$	+1.09		+1.47	-0.03	+0.49	
$[(^{Me2}TACN\text{-}Py_2)Fe^{IV}(O)]^{2+}$	+0.95		+1.23	-0.18		
$[(BP1)Fe^{IV}(O)]^{2+}$	+1.12		+1.38	-0.08		
$[(BP2)Fe^{IV}(O)]^{2+}$	+1.17		+1.63	+0.12		
$[(TMC)Fe^{IV}(O)(CH_3CN)]^{2+}$					+0.39	
$[(TMC)Fe^{IV}(O)\{OC(O)CF_3\}]^{+}$					+0.13	
$[(TMC)Fe^{IV}(O)(N_3)]^{+}$					-0.05	

[a]Corresponding Fe(II) complexes, [b]spectropotentiometric titrations starting with corresponding Fe(II) complexes, from Reference (23), [c]from Reference (25), [d]starting with Fe^{IV}=O complexes from Reference (23), [e]starting with Fe^{IV}=O complexes from Reference (28), [f]starting with Fe^{IV}=O complexes from Reference (27) and all potentials are *vs.* SCE.

Determining the Fe^{IV}/Fe^{III} potential is evidently not straightforward as will be shown in the chapter 4 due to their slow rates of heterogeneous electron transfer, which limits the usefulness of direct measurement by cyclic voltammetry. The reduction potential of the Fe^{IV}/Fe^{III}(O) couple has also been determined by the titration with one electron reductants such as ferrocene and its derivatives. It is important to note that this approach requires that the redox couple is reversible electrochemically.

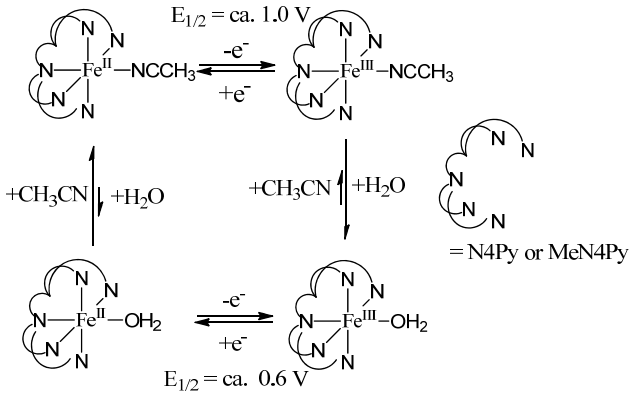

Figure 8 Species and equilibria occurring in aqueous/acetonitrile mixtures for $[(N4Py)Fe^{II}(CH_3CN)]^{2+}$.[25]

Figure 8 shows the equilibria that exists between various species in acetonitrile/water for $[(N4Py)Fe^{II}(CH_3CN)]^{2+}$. A potential of +1.1 V *vs.* SCE is required to generate the Fe^{III}-CH_3CN species from Fe^{III}-CH_3CN, whereas only at most +0.6 V *vs.* SCE is needed to generate Fe^{III}-OH_2 from Fe^{II}-OH_2. The need for highly positive potentials to generate the Fe(III) species in acetonitrile is possibly the reason why identifying the oxidation potential of the Fe^{IV}/Fe^{III} couple is troublesome (Figure 9).[25,26] First Fe^{III}-CH_3CN must be generated from Fe^{II}-CH_3CN at +1.01 V *vs.* SCE. If water is present, immediate ligand exchange occurs to form Fe^{III}-OH, which can then be oxidised at +1.01 V or less *vs.* SCE. However, the potential must be held at above +1.01 V to complete both steps (see chapter 4).

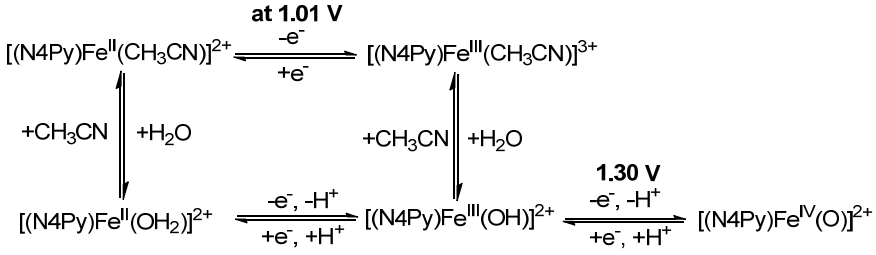

Figure 9 Redrawn from reference 26.

To avoid this problem water is the solvent of choice because of the lower potential needed to oxidize Fe(II) to Fe(III) (+0.6 V *vs.* SCE). Even though a reversible redox wave assigned to the Fe^{IV}/Fe^{III} couple in water was assigned to the $[(N4Py)Fe^{IV}(O)]^{2+}$ reduction, this assignment is questionable, due to the overlap of $Fe^{III}/Fe^{II}(OH/H_2O)$ redox wave and the role of catalytic processes at the electrodes. Spectropotentiometric titrations in water would be expected to give a better handle

to assign the oxidation potential of $Fe^{IV}/Fe^{III}(O)$ couple since the signal (absorption) is not dependent on time in the same way current is and, hence, slow heterogeneous electron transfer rates are less of an issue. In chapter 4 the question of the redox potentials of Fe^{IV}=O species will be addressed.

I.3 Biochemical halogenation reactions

Halocarbons are frequent structural motifs in many marine natural products, including antibiotics and hormones and compounds of pharmaceutical and agrichemical interest,[29] and are key precursors in organic synthesis. Contemporary synthetic methods for late stage incorporation of halogens into complex systems are often hampered by a lack of selectivity and specificity, however. Nature, by contrast, uses haloperoxidases and halogenases to achieve this in a highly specific and selective manner[30,31] and hence biomimetic functional approaches offer substantial promise in this regard. Several haloperoxidases have been characterised by means of X-ray crystallography.[32] Based on their requirement for oxygen based oxidants for halogenation of the substrates they can be divided into two classes, (1) haloperoxidase and (2) halogenases.[30] Both, Vanadium and heme dependent enzymes use hydrogen peroxide as oxidant to generate the active intermediates for halogenation reactions and hence they are called haloperoxidases also. In contrast non-heme and flavin dependent enzymes use molecular oxygen as oxidant to generate the corresponding active intermediates towards halogenation of substrates, are named halogenases.

I.3.1 Halogenases

I.3.1.1 Flavin dependent halogenases

This class of enzymes does not contain a metal center in their structure. PrnA (tryptophan 7-halogenase) and PrnC are examples of flavin dependent halogenases. The chlorination reactions catalysed by this family of enzymes are highly regiospecific. Due to the high regiospecificity of these enzymes, involvement of free HOCl in the reactions is excluded. These enzymes use X^+ (X = Cl or Br) equivalents to halogenate electron rich substrates. The mechanism suggested by van Pée (via a 4α-hydroperoxyflavin intermediate)[33] and Walsh (via a FAD-4α-OCl intermediate)[34] were later shown to be unlikely when the crystal structure of PrnA (with FAD, tryptophan and chloride bound) was reported by Naismith.[35]

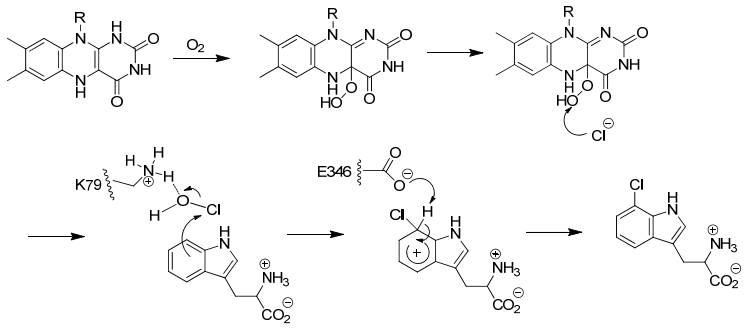

Scheme 1 Naismith mechanism (production of HOCl followed by protein mediated electrophilic aromatic substitution). Redrawn figure from References 30 and 36.

Indeed halogenation involves HOCl but FAD exerts substantial control over HOCl by keeping it within the channel through hydrogen bonding. The proposed catalytic path is shown in scheme 1.[36] Activated FAD reacts with molecular oxygen and generates the species FAD-OOH. Chloride (Cl^-) then attacks FAD-OOH to form the FAD-OH (not shown in scheme 1) and HOCl. The K79 residue forms hydrogen bonds with HOCl to keep it within the channel. Electrophilic attack of the hypochlorous acid (Cl^+ equivalent) on tryptophan C7 forms the carbocationic intermediate. Deprotonation of the carbocation proceeds by the E346 residue resulting in chlorination of tryptophan.[37]

I.3.1.2 Non-heme iron dependent halogenases

As mentioned above this class of enzymes uses non-heme Fe(II)/α-ketoglutarate and oxygen to perform the halogenation of the inert aliphatic C-H bonds.[30] SyrB1 and CmaA are a few examples of this class of halogenases. The key difference between the non-heme Fe(II)/αKG dependent hydrolase and non-heme Fe(II)/αKG dependent halogenase is that the latter contains a chlorido ligand instead of an aspartate moiety.[30,38]

The reaction cycle of non-heme Fe(II)/αKG dependent halogenase with aliphatic C-H substrates is presented in scheme 2.[38] In the presence of the substrate ($R\text{-}CH_3$), the aqua ligand on the Fe(II) complex dissociates to facilitate the coordination of molecular oxygen. The Fe^{IV}=O intermediate that forms upon decarboxylation has been characterised by Mössbauer and (resonance)Raman spectroscopy. The highly reactive Fe^{IV}=O intermediate can attack the C-H group in the substrate and form a Cl-Fe^{III}-OH intermediate and an alkyl radical. In contrast to non-heme Fe(II)/αKG dependent hydrolase, a chlorine radical ($Cl^{\cdot}$) reacts with an alkyl radical ($R\text{-}CH_2^{\cdot}$) and leads to the formation of chlorinated products.[38] At this stage hydroxy ($^{\cdot}OH$)

radicals can compete with chloride radicals. The formation of the hydroxy radicals is thermodynamically unfavourable compare to chloride radicals.[32d,39] In contrast to flavin dependent halogenases, these enzymes use $X^{\cdot}$ (X = Cl or Br) equivalents to halogenate at aliphatic C-H positions.

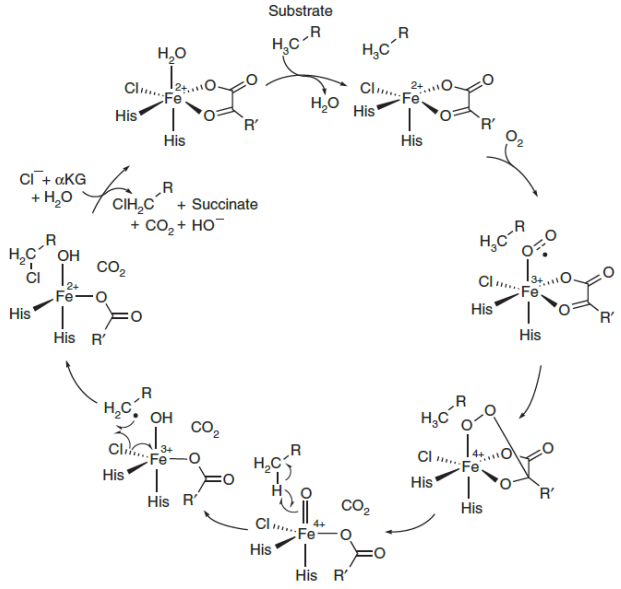

Scheme 2 Proposed mechanism of the Fe(II)- and αKG-dependent halogenases. R = -CH_2-L-CH(NH_2)-CO-S-CytC2; R' = -$(CH_2)_2CO_2$-. Reproduced from Reference 38.

I.3.2 Haloperoxidases

I.3.2.1 Vanadium dependent haloperoxidases

Among the vanadium dependent haloperoxidases, vanadium bromo peroxidase is well known due to its potential involvement in the biosynthesis of number of halogenated natural products.[40] In this class of enzymes an imidazole ring from a histidine residue is ligated to the vanadium ion.[30] Vanadium dependent haloperoxidases use vanadate, hydrogen peroxide and halide (Cl^-, Br^- and I^-) for the halogenation of the electron rich substrates.[41] The catalytic cycle and the intermediates generated by this class of enzymes are shown in scheme 3. The reaction between the vanadium complex and H_2O_2 produces a side-on peroxy species, which will then attack the halide ion. Two electron oxidation of the halide ion by peroxy species generates a V-O-X adduct. The exact nature of the halogenating species in vanadium dependent haloperoxidases is not clear. As with flavin dependent halogenases and heme dependent haloperoxidases, these enzymes use X^+ (X = Cl, Br and I) equivalents to halogenate the electron rich substrates with

varying degrees of stereo-specificity and regioselectivity.

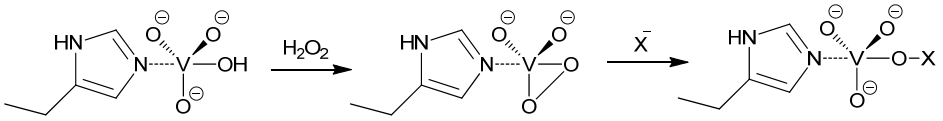

Scheme 3 Vanadium-dependent haloperoxidases. Redrawn from Reference 30.

I.3.2.2 Heme dependent haloperoxidases

Heme dependent haloperoxidases use hydrogen peroxide and halide ions to halogenate substrates. Chloroperoxidase (CPO) from *Caldariomyces fumago*,[42] myeloperoxidase (MPO), Thyroid peroxidase (TPO), lactoperoxidase (LPO) and eosinophil peroxidase (EPO) are a few examples of heme dependent halo peroxidases. As with flavin dependent halogenase, heme dependent halo peroxidases use X^+ (X = Cl or Br) equivalents for the halogenation reactions, so this class of enzymes engage in halogenation of electron rich substrates. The intermediates and the proposed catalytic cycle is shown in scheme 3. Initially, heme Fe(III) reacts with hydrogen peroxide, which generates the high valent $^{+\bullet}$heme-Fe^{IV}=O species known as Compound I.[43,44] Then Compound I oxidizes the halide ion by two electrons and forms the heme-Fe^{III}-O-X (where X = Cl, Br and I) adduct.[44] It was proposed that the OX^- bound metal complex is responsible for the halogenation, but the actual structure of the chlorinating agent is still matter of debate.

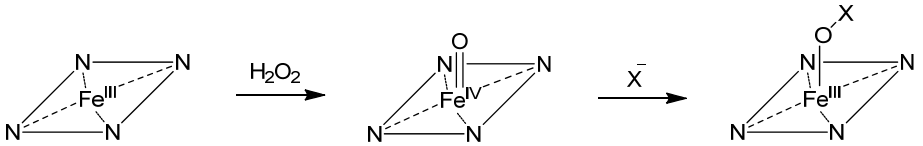

Scheme 4 Intermediates in the mechanism of heme-dependent halogenation reaction. Redrawn from Reference 30.

Even though the participation of a heme-Fe^{III}-OCl adduct is proposed in the catalytic cycle of heme dependent haloperoxidases, direct spectroscopic evidence for heme-Fe^{III}-OCl adduct was observed only recently by Hiroshi et al.[45] Addition of OCl^- to [(TPFP)Fe^{III}(OH)] in CH_3CN/CH_2Cl_2 generates an intermediate assigned as [(TPFP)$Fe^{III}(OCl)_2]^-$. Characterization of this intermediate was carried out by (resonance)Raman, EPR and NMR spectroscopy and by ESI-MS. This intermediate is stable for 1 h at -60 °C and decomposes to [(TPFP)Fe^{IV}(O)]. This is the first evidence and spectroscopic characterisation of a Fe^{III}-OCl species (M = Mn, Fe, Ni) for a porphyrinic systems. To the best of my knowledge, evidence for the formation

of the M-OCl adducts and their potential role in catalysis (C-H bond chlorination and oxygenation and epoxidation of alkenes) has not been reported in any of the non-heme and non-porphyrinic systems. Synthesis and spectroscopic characterisation of haloperoxidase mimics such as non-heme iron and non-porphyrinic nickel complexes and their reactions with NaOCl are discussed in chapter 6 and 7.

I.4 Ligand Names

(1) TPA = tris(2-pyridylmethyl)amine
(2) TMC = 1,4,8,11-tetramethyl-1,4,8,11-tetraazacyclotetradecane
(3) N4Py = bis(2-pyridylmethyl)bis(2-pyridyl)methylamine
(4) Bn-TPEN = *N*-benzyl-*N*,*N*',*N*'-tris(2-pyridylmethyl)-1,2-diaminoethane
(5) Me-TPEN = *N*-methyl-*N*,*N*',*N*'-tris(2-pyridylmethyl)-1,2-diaminoethane
(6) Me-TPPN = *N*-methyl-*N*,*N*',*N*'-tris(2-pyridylmethyl)-1,3-diaminopropane
(7) BPMCN = *N*,*N*'-bis(2-pyridylmethyl)- *N*,*N*'-dimethyltrans-1,2-diaminocyclohexane
(8) [H_3buea] = tris[(*N*'-tertbutylureaylato)-*N*-ethyl]aminato
(9) BQCN=*N, N*'-dimethyl-*N, N*'-bis(8-quinolyl)cyclohexanediamine
(10) TPEN = *N,N,N*',*N*'-tetrakis(2-pyridylmethyl)ethane-1,2-diamine
(11) trispicmeen = *N*-methyl-*N,N',N*'-tris(2-pyridylmethyl)ethane-l,2-diamine
(12) trispicen = [*N,N*',*N*'-tris(2-pyridylmethyl)ethane-1,2-diamine
(13) [15]aneN_4 = 1,4,8,12-Tetraazacyclopentadecane
(14) PY5 = 2,6-bis-((2-pyridyl)methoxymethane)pyridine
(15) OEP = octaethylporphyrin dianion, TPP = tetraphenylporphyrin dianion
(16) Hbppa = *N*-(2-pyridylmethyl)bis(6-pivalamido-2-pyridylmethyl)amine
(17) L^8py_2 = *N,N*'-bis(2-pyridylmethyl)-1,5-diazacyclooctane
(18) Tp^{iPr2} = HB(pz′)$_3$, where pz′ is 3,5-bis(isopropyl)pyrazolyl
(19) 6-Me_2BPP = *N*,*N*-bis(6-methyl-2-pyridylmethyl)-3-aminopropionate
(20) *N*-Et-HPTB=*N*,*N*,*N*′,*N*′-tetrakis(1′-ethylbenzimidazolyl-2′-methyl)-2-hydroxy-1,3-diaminopropane
(21) Me-BQPA = Bis(2-quinolylmethyl)-6-methylpyridyl-2-methylamine
(22) H_4EDTA = *N*,*N*′-ethylenebis(N-(carboxymethyl)glycine)
(23) HPTB = *N*,*N*,*N*',*N*′-tetrakis(2-benzimidazolylmethyl)-2-hydroxy-l,3-diaminopropane
(24) TBC = 1,4,8,11-tetrabenzyl-1,4,8,11-tetraazacyclotetradecane
(25) salen = 2,2'-Ethylenebis(nitrilomethylidene)diphenol
(26) H_3TTPPC = 5,10,15- tris(2,4,6-triphenylphenyl)-corrole
(27) TBP = 4-*tert*-butylphenyl
(28) [14]ane = Cyclam = 1,4,8,1l-tetraazacyclotetradecane
(29) OEP = octaethylporphyrin

I.5 References

(1) F. H. Tukhvatullin, A. K. Atakhodjev, A. Djumabaev, U. N. Tashkenbaev, I. P. Kleiner, S. A. Osmanov, *J. Mol. Liq.*, **1992**, *64*, 19-25.
(2) C. Brennan, A. Draksharapu, W. R. Browne, J. J. McGarvey, J. G. Vos, M.T. Pryce, *Dalton Trans.*, **2013**, *42*, 2546-2555.
(3) (a) R. Y. N. Ho, L. Que, Jr., *Chem Rev.,* **1996**, *96*, 2607-2624; (b) E. I. Solomon, T. C. Brunold, M. I. Davis, J. N. Kemsley, S. K. Lee, N. Lehnert, F. Neese, A. J. Skulan, Y. S. Yang, J. Zhou, *Chem Rev.,* **2000**, *100*, 235-349; (c) A. L. Feig, S. J. Lippard, *Chem Rev.,* **1994**, *94*, 759-805; (d) B. J. Wallar, J. D. Lipscomb, *Chem Rev*., **1996**, *96*, 2625-2657; (e) M. Merkx, D. A. Kopp, M. H. Sazinsky, J. L. Blazyk, J. Muller, S. J. Lippard, *Angew. Chem., Int. Ed.,* **2001**, *40*, 2782-2807; (f) J. T. Groves, In Cytochrome P450: Structure, Mechanism, and Biochemistry, 3rd ed. (Ed.: P. R. Ortiz de Montellano), Kluwer Academic/Plenum Publishers, New York, **2005**, pp. 1-43; (g) J. P. McEvoy, G. W. Brudvig, *Chem. Rev*., **2006**, *106*, 4455-4483; (h) B. Meunier, A. Robert, G. Pratviel, J. Bernadou in The Porphyrin Handbook, Vol. 4 (Eds.: K. M. Kadish, K. M. Smith, R. Guilard), Academic Press, San Diego, **2000**, pp. 119-187.
(4) A. S. Borovik, *Chem. Soc. Rev*., **2011**, *40*, 1870-1874.
(5) E. Y. Tshuva, S. J. Lippard, *Chem. Rev.,* **2004**, *104,* 987-1012.
(6) (a) H. Umezawa, K. Maeda, T. Takeuchi, Y. Okami, *J. Antibiot.,* **1966**, *19*, 200-209; (b) S. M. Hecht, Bleomycin: Chemical, Biochemical and Biological Aspects; Springer: New York, **1979**; (c) R. M. Burger, *Chem. Rev.,* **1998**, *98*, 1153-1169; (d) C. A. Claussen, E. C. Long, *Chem. Rev.,* **1999**, *99*, 2797-2816; (e) S. M. Hecht, *J. Nat. Prod.,* **2000**, *63*, 158-168.
(7) J. W. Sam, X. -J. Tang, J. Peisach, *J. Am. Chem. Soc*., **1994**, *116*, 5250-5256.
(8) (a) M. Lubben, A. Meetsma, E. C. Wilkinson, B. L. Feringa, L. Que, Jr., *Angew. Chem. Int. Ed. Engl.,* **1995**, *34*, 1512-1514; (b) G. Roelfes, M. E. Branum, L. Wang, L. Que, Jr., B. L. Feringa, *J. Am. Chem. Soc.,* **2000**, *122*, 11517-11518; (c) T. A. van den Berg, B. L. Feringa, G. Roelfes, *Chem. Commun.,* **2007**, 180-182; (d) R. P. Megens, T. A. van den Berg, A. D. de Bruijn, B. L. Feringa, G. Roelfes, *Chem. -Eur. J.,* **2009**, *15*, 1723-1735; (e) Q. Li, T. A. van den Berg, B. L. Feringa, G. Roelfes, *Dalton Trans.*, **2010**, 8012-8021; (f) Q. Li, W. R. Browne, G. Roelfes, *Inorg. Chem.*, **2010**, *49*, 11009-10017.
(9) R. Y. N. Ho, G. Roelfes, R. Hermant, R. Hage, B. L. Feringa, L. Que, Jr., *J. Am. Chem. Soc.,* **1999**, *121*, 264-265.
(10) (a) G. Roelfes, V. Vrajmasu, K. Chen, R. Y. N. Ho, J. Rohde, C. Zondervan, R. M. la Crois, E. P. Schudde, M. Lutz, A. L. Spek, R. Hage, B. L. Feringa, E. Münck, L. Que, Jr., *Inorg. Chem.*, **2003**, *42*, 2639-2653; (b) M. P. Jensen, A. Mairata i Payeras, A. T. Fiedler, M. Costas, J. Kaizer, A. Stubna, E. Münck, L. Que, Jr., *Inorg. Chem.*, **2007**, *46*, 2398-2408; (c) M. P. Jensen, M. Costas, R. Y. Ho, N. J. Kaizer, A. Mairata i Payeras, E. Munck, L. Que, Jr., U. Rohde, A. Stubna, *J. Am. Chem. Soc.*, **2005**, *127*, 10512-10525; (d) T. Kojima, K. Nakayama, M. Sakaguchi, T. Ogura, K. Ohkubo, S. Fukuzumi, *J. Am. Chem. Soc.*, **2011**, *133*, 17901-17911; (e) Y. Zang, J. Kim, Y. Dong, E. C. Wilkinson, E. H. Appelman, L. Que, Jr., *J. Am. Chem. Soc.*, **1997**, *119,* 4197-4205; (f) A. J. Simaan, S. Döpner, F. Banse, S. Bourcier, G. Bouchoux, A. Boussac, P. Hildebrandt, J. -J. Girerd, *Eur. J. Inorg. Chem.*, **2000**, 1627-1633; (g) I. Bernal, I. M. Jensen, K. B. Jensen, C. J. McKenzie, H. Toftlund, J. P. Tuchagues, *J. Chem. Soc., Dalton Trans.*, **1995**, 3667-3675; (h) F. Namuswe, G. D. Kapser, A. A. N. Sarjeant, C. Krest, T. Hayashi, M. T. Green, P. Moenne-Loccoz, D. P. Goldberg, *J. Am. Chem. Soc*., **2008**, *130*, 14189-14200; (i) S. Menage, E. C. Wilkinson, L. Que, Jr., M. Fontecave, *Angew. Chem. Int. Ed.,* **1995**, *34*, 203-205; (j) A. Wada, S. Ogo, S. Nagatomo, T. Kitagawa, Y. Watanabe, K. Jitsukawa, H. Masuda, *Inorg. Chem.*, **2002**, *41*, 616-618; (k) M. R. Bukowski, H. L. Halfen, T. A. van der Berg, J. A. Halfen, L. Que, Jr., *Angew. Chem. Int. Ed.*, **2005**, *44*, 584-587; (l) Y. Zang, T. E. Elgren, Y. Dong, L. Que, Jr., *J. Am. Chem. Soc.*, **1993**, *115*, 811-813.

(11) (a) J. Cho, S. Jeon, S. A. Wilson, L. V. Liu, E. A. Kang, J. J. Braymer, M. H. Lim, B. Hedman, K. O. Hodgson, J. S. Valentine, E. I. Solomon, W. Nam, *Nature,* **2011**, *478*, 502-505; (b) S. Fukuzumi, Y. Morimoto, H. Kotani, P. Naumov, Y. -M. Lee, W. Nam, *Nat. Chem.,* **2010**, 2, 756-759.
(12) (a) E. McCandlish, A. R. Miksztal, M. Nappa, A. Q. Sprenger, J. S. Valentine, J. D. Stong, T. G. Spiro, *J. Am. Chem. Soc.,* **1980**, *102*, 4268-4271; (b) S. Ahmad, J. D. McCallum, A. K. Shiemke, E. H. Appelman, T. M. Loehr, J. Sanders-Loehr, *Inorg. Chem.,* **1988**, *27*, 2230-2233.
(13) K. M. Van Heuvelena, A. T. Fiedlera, X. Shana, R. F. De Hontc, K. K. Meierc, E. L. Bominaarc, E. Münck, L. Que, Jr., *Proc. Acad. Sci. USA*, **2012**, *109*, 11933-11938.
(14) (a) C. E. MacBeth, A. P. Golombek, V. G. Young, Jr., C. Yang, K. Kuczera, M. P. Hendrich, A. S. Borovik, *Science,* **2000**, *289*, 938-941; (b) H. -Y. Liu, F. Yam, Y. T. Xie, X. Y. Li, C. K. Chang, *J. Am. Chem. Soc.,* **2009**, *131*, 12890-12891; (c) C. E. MacBeth, R. Gupta, K. R. Mitchell-Koch, V. G. Young, Jr., G. H. Lushington, W. H. Thompson, M. P. Hendrich, A. S. Borovik, *J. Am. Chem. Soc.,* **2004**, *126*, 2556-2567; (d) S. C. Sawant, X. Wu, J. Cho, K. -B. Cho, S. H. Kim, M. S. Seo, Y. -M. Lee, M. Kubo, T. Ogura, S. Shaik, W. Nam, *Angew. Chem. Int. Ed.*, **2010**, *49*, 1-6; (e) Y. Shimazaki, T. Nagano, H. Takesue, B. -H. Ye, F. Tani, Y. Naruta, *Angew. Chem. Int. Ed.,* **2004**, *43*, 98-100; (f) Y. Hirai, T. Kojima, Y. Mizutani, Y. Shiota, K. Yoshizawa, S. Fukuzumi, *Angew. Chem. Int. Ed.,* **2008**, *47*, 5772-5776; (f) C. V. Sastri, M. J. Park, T. Ohta, T. A. Jackson, A. Stubna, M. S. Seo, J. Lee, J. Kim, T. Kitagawa, E. Münck, L. Que, Jr., W. Nam, *J. Am. Chem. Soc.,* **2005**, *127*, 12494-12495; (g) M. Martinho, F. Banse, J. -F. Bartoli, T. A. Mattioli, P. Battioni, O. Horner, S. Bourcier, J. -J. Girerd, *Inorg. Chem.,* **2005**, *44*, 9592-9596; (h) A. Thibon, J. England, M. Martinho, V. G. Young, Jr., J. R. Frisch, R. Guillot, J. -J. Girerd, E. Münck, L. Que, Jr., F. Banse, *Angew. Chem. Int. Ed.,* **2008**, *47*, 7064-7067; (i) Y. -M. Lee, S. N. Dhuri, S. C. Sawant, J. Cho, M. Kubo, T. Ogura, S. Fukuzumi, W. Nam, *Angew. Chem. Int. Ed.,* **2009**, *121*, 1835-1838; (j) S. A. Wilson, J. Chen, S. Hong, Y. -M. Lee, M. Clémancey, R. Garcia-Serres, T. Nomura, T. Ogura, J. -M. Latour, B. Hedman, K. O. Hodgson, W. Nam, E. I. Solomon, *J. Am. Chem. Soc.*, 2012, *134*, 11791-11806; (k) L. M. Proniewicz, K. Bajdor, K. Nakamoto, *J. Phys. Chem.,* **1986**, *90*, 1760-1766; (l) T. J. Collins, R. D. Powell, C. Slebodnick, E. S. Uffelman, *J. Am. Chem. Soc.,* **1990**, *112*, 899-901.
(15) N. Jin, M. Ibrahim, T. G. Spiro, J. T. Groves, *J. Am. Chem. Soc.*, **2007**, *129*, 12416-12417.
(16) (a) Y. Dong, Y. Zang, K. Kauffmann, L. Shu, E. C. Wilkinson, E. Münck, L. Que, Jr., *J. Am. Chem. Soc.,* **1997**, *119*, 12683-12684; (b) A. T. Fiedler, X. Shan, M. P. Mehn, J. Kaizer, S. Torelli, J. R. Frisch, M. Kodera, L. Que, Jr., *J. Phys. Chem. A,* **2008**, *112*, 13037-13044; (c) X. Zhang, H. Furutachi, S. Fujinami, S. Nagatomo, Y. Maeda, Y. Watanabe, T. Kitagawa, M. Suzuki, *J. Am. Chem. Soc.,* **2005**, *127*, 826-827; (d) N. Kitajima, N. Tamura, H. Amagai, H. Fukui, Y. Moro-oka, Y. Mizutani, T. Kitagawa, R. Mathur, K. Heerwegh, C. A. Reed, C. R. Randall, L. Que, Jr., K. Tatsumi, *J. Am. Chem. Soc.,* **1994**, *116*, 9071-9085; (e) K. Kim, S. J. Lippard, *J. Am. Chem. Soc.,* **1996**, *118*, 4914-4915.
(17) D. M. Kurtz, Jr., *Chem. Rev.,* **1990***, 90,* 585-606.
(18) M. Murakami, D. Hong, T. Suenobu, S. Yamaguchi, T. Ogura, S. Fukuzumi, *J. Am. Chem. Soc.*, **2011**, *133*, 11605-11613.
(19) A. S. Borovik, *Acc. Chem. Res*., **2005**, *38*, 54-61.
(20) T. H. Parsell, R. K. Behan, M. T. Green, M. P. Hendrich, A. S. Borovik, *J. Am. Chem. Soc*., **2006**, *128*, 8728-8729.
(21) T. Taguchi, R. Gupta, B. Lassalle-Kaiser, D. W. Boyce, V. K. Yachandra, W. B. Tolman, J. Yano, M. P. Hendrich, A. S. Borovik, *J. Am. Chem. Soc*., **2012**, *134*, 1996-1999.
(22) http://www.nobelprize.org/nobel_prizes/chemistry/laureates/1913/ on 20130922.
(23) D. Wang, K. Ray, M. J. Collins, E. R. Farquhar, J. R. Frisch, L. Gómez, T. A. Jackson, M. Kerscher, A. Waleska, P. Comba, M. Costas, L. Que, Jr., *Chem. Sci.*, **2013**, *4*, 282-291.
(24) S. Fukuzumi, *Coord. Chem. Rev.*, **2013**, *257*, 1564-1575.

(25) A. Draksharapu, Q. Li, H. Logtenberg, T. A. van den Berg, A. Meetsma, J. S. Killeen, B. L. Feringa, R. Hage, G. Roelfes, W. R. Browne, *Inorg. Chem*., **2012**, *51,* 900-913.
(26) M. J. Collins, K. Ray, L. Que, Jr., *Inorg. Chem.*, **2006**, *45*, 8009-8011.
(27) D. Wang, M. Zhang, P. Bühlmann, L. Que, Jr., *J. Am. Soc.*, **2010**, *132*, 7638-7644.
(28) Y. -M. Lee, H. Kotani, T. Suenobu, W. Nam, S. Fukuzumi, *J. Am. Chem. Soc.*, **2008**, *130*, 434-435.
(29) (a) G. W. Gribble, *Acc. Chem. Res.*, **1998**, *31*, 141-152; (b) K. H. van Pée, C. J. Dong, S. Flecks, J. Naismith, E. P. Patallo, T. Wage, *Adv. Appl. Microbiol.*, **2006**, *59*, 127-157; (c) J. H. Dawson, M. Sono, *Chem. Rev.,* **1987**, *87*, 1255-1276; (d) L. P. Hager, D. R. Morris, F. S. Brown, H. Eberwein, *J. Biol. Chem.*, **1966**, *241*, 1769-1777; (e) S. R. Blanke, L. P. Hager, *J. Biol. Chem.*, **1988**, *263*, 18739-18743.
(30) F. H. Vaillancourt, E. Yeh, D. A. Vosburg, S. G. -Tsodikova, C. T. Walsh, *Chem. Rev.*, **2006**, *106*, 3364-3378.
(31) A. Podgoršek, M. Zupan, J. Iskra, *Angew. Chem. Int. Ed.*, **2009**, *48*, 8424-8450.
(32) (a) C. Dong, S. Flecks, S. Unversucht, C. Haupt, K. -H. van Pée, J. H. Naismith, *Science*, **2005**, *309*, 2216-2218; (b) M. Weyand, H. -J. Hecht, M. Kieß, M. -F. Liaud, H. Vilter, D. Schomburg, *J. Mol. Biol.*,**1999**, *293*, 595-611; (c) M. N. Isupov, A. R. Dalby, A. A. Brindley, Y. Izumi, T. Tanabe, G. N. Murshudov, J. A. Littlechild, *J. Mol. Biol.*, **2000**, *299*, 1035-1049; (d) L. C. Blasiak, F. H. Vaillancourt, C. T. Walsh, C. L. Drennan, *Nature*, **2006**, *440*, 368-371.
(33) (a) S. Keller, T. Wage, K. Hohaus, M. Hölzer, E. Eichhorn, K. -H. van Pée, *Angew. Chem. Int. Ed.*, **2000**, *39*, 2300-2301; (b) K. -H. van Pée, *Annu. Rev. Microbiol.*, **1996**, *50*, 375-399.
(34) (a) E. Yeh, S. Garneau, C. T. Walsh, *Proc. Natl. Acad. Sci. USA*, **2005**, *102*, 3960-3965; (b) P. Dorrestein, E. Yeh, S. G. -Tsodikova, N. L. Kelleher, C. T. Walsh, *Proc. Natl. Acad. Sci. USA*, **2005**, *102*, 13843-13848.
(35) C. Dong, A. Kotzsch, M. Dorward, K. -H. van Pée, J. H. Naismith, *Acta Crystallogr., Sect. D: Biol. Crystallogr.*, **2004**, *60*, 1438-1440.
(36) J. L. Ross Anderson, S. K. Chapman, *Mol. BioSyst.*, **2006**, *2*, 350-357.
(37) J. H. Naismith, *Chem. Soc. Rev.,* **2006**, *35*, 763-770.
(38) D. P. Galonic, E. W. Barr, C. T. Walsh, J. M. Bollinger, Jr., C. Krebs, *Nat. Chem. Biol.,* **2007**, *3*, 113-116.
(39) T. Kojima, R. A. Leising, S. Yan, L. Que, Jr., *J. Am. Chem. Soc.*, **1993**, *115*, 11328-11335.
(40) (a) A. Butler, *Curr. Opin. Chem. Biol.,* **1998**, *2*, 279-285; (b) J. S. Martinez, G. L. Carroll, R. A. Tschirret-Guth, G. Altenhoff, R. D. Little, A. Butler, *J. Am. Chem. Soc.*, **2001**, *123,* 3289-3294.
(41) A. Butler, J. V. Walker, *Chem. Rev.*, **1993**, *93*, 1937-1944.
(42) K. Welinder, *Curr. Opin. Struct. Biol.*, **1992**, *2*, 388-393.
(43) H. A. Wagenknecht, W. D. Woggon, *Chem. Biol.,* **1997**, *4*, 367-372.
(44) K. L. Stone, R. K. Behan, M. T. Green, *Proc. Natl. Acad. Sci. U.S.A.,* **2005**, *102*, 16563-16565.
(45) Z. Cong, S. Yanagisawa, T. Kurahashi, T. Ogura, S. Nakashima, H. Fujii, *J. Am. Chem. Soc.*, **2012**, *134*, 20617-20620.